Evidence for frequency comb emission from a Fabry-Pérot terahertz quantum-cascade laser

M. Wienold,* B. Röben, L. Schrottke, and H. T. Grahn

Paul-Drude-Institut für Festkörperelektronik, Hausvogteiplatz 5–7, 10117 Berlin, Germany

* *wienold@pdi-berlin.de*

Abstract: We report on a broad-band terahertz quantum-cascade laser (QCL) with a long Fabry-Pérot ridge cavity, for which the tuning range of the individual laser modes exceeds the mode spacing. While a spectral range of approximately 60 GHz (2 cm^{-1}) is continuously covered by current and temperature tuning, the total emission range spans more than 270 GHz (9 cm^{-1}). Within certain operating ranges, we found evidence for stable frequency comb operation of the QCL. An experimental technique is presented to characterize frequency comb operation, which is based on the self-mixing effect.

OCIS codes: (140.5965) Semiconductor lasers, quantum cascade; (140.3070) Infrared and far-infrared lasers.

References and links

1. H.-W. Hübers, S. G. Pavlov, A. D. Semenov, R. Köhler, L. Mahler, A. Tredicucci, H. E. Beere, D. A. Ritchie, and E. H. Linfield, "Terahertz quantum cascade laser as local oscillator in a heterodyne receiver," Opt. Express **13**, 5890–5896 (2005).
2. J. L. Kloosterman, D. J. Hayton, Y. Ren, T. Y. Kao, J. N. Hovenier, J. R. Gao, T. M. Klapwijk, Q. Hu, C. K. Walker, and J. L. Reno, "Hot electron bolometer heterodyne receiver with a 4.7-THz quantum cascade laser as a local oscillator," Appl. Phys. Lett. **102**, 011123 (2013).
3. R. Eichholz, H. Richter, S. G. Pavlov, M. Wienold, L. Schrottke, R. Hey, H. T. Grahn, and H.-W. Hübers, "Multi-channel terahertz grating spectrometer with quantum-cascade laser and microbolometer array," Appl. Phys. Lett. **99**, 141112 (2011).
4. L. Consolino, S. Bartalini, H. E. Beere, D. A. Ritchie, M. S. Vitiello, and P. De Natale, "THz QCL-based cryogen-free spectrometer for in situ trace gas sensing," Sensors **13**, 3331–3340 (2013).
5. N. Rothbart, H. Richter, M. Wienold, L. Schrottke, H. T. Grahn, and H.-W. Hübers, "Fast 2-D and 3-D terahertz imaging with a quantum-cascade laser and a scanning mirror," IEEE Trans. Terahertz Sci. Technol. **3**, 617–624 (2013).
6. P. Dean, Y. L. Lim, A. Valavanis, R. Kliese, M. Nikolić, S. P. Khanna, M. Lachab, D. Indjin, Z. Ikonić, P. Harrison, A. D. Rakić, E. H. Linfield, and A. G. Davies, "Terahertz imaging through self-mixing in a quantum cascade laser," Opt. Lett. **36**, 2587–2589 (2011).
7. M. Ravaro, V. Jagtap, G. Santarelli, C. Sirtori, L. H. Li, S. P. Khanna, E. H. Linfield, and S. Barbieri, "Continuous-wave coherent imaging with terahertz quantum cascade lasers using electro-optic harmonic sampling," Appl. Phys. Lett. **102**, 091107 (2013).
8. L. Werner, H.-W. Hübers, P. Meindl, R. Müller, H. Richter, and A. Steiger, "Towards traceable radiometry in the terahertz region," Metrologia **46**, S160–S164 (2009).
9. H. Richter, M. Greiner-Bär, S. G. Pavlov, A. D. Semenov, M. Wienold, L. Schrottke, M. Giehler, R. Hey, H. T. Grahn, and H.-W. Hübers, "A compact, continuous-wave terahertz source based on a quantum-cascade laser and a miniature cryocooler," Opt. Express **18**, 10177–10187 (2010).
10. M. I. Amanti, G. Scalari, M. Beck, and J. Faist, "Stand-alone system for high-resolution, real-time terahertz imaging," Opt. Express **20**, 2772–2778 (2012).
11. A. Hugi, G. Villares, S. Blaser, H. C. Liu, and J. Faist, "Mid-infrared frequency comb based on a quantum cascade laser," Nature **492**, 229–233 (2012).

#214514 - $15.00 USD Received 6 Aug 2014; revised 2 Oct 2014; accepted 18 Nov 2014; published 1 Dec 2014

12. D. Burghoff, T.-Y. Kao, N. Han, C. W. I. Chan, X. Cai, Y. Yang, D. J. Hayton, J.-R. Gao, J. L. Reno, and Q. Hu, "Terahertz laser frequency combs," Nat. Photonics **8**, 462–467 (2014).
13. Th. Udem, R. Holzwarth, and T. W. Hänsch, "Optical frequency metrology," Nature **416**, 233–237 (2002).
14. J. Mandon, G. Guelachvili, and N. Picqué, "Fourier transform spectroscopy with a laser frequency comb," Nat. Photonics **3**, 99–102 (2009).
15. M. S. Vitiello, L. Consolino, S. Bartalini, A. Taschin, A. Tredicucci, M. Inguscio, and P. De Natale, "Quantum-limited frequency fluctuations in a terahertz laser," Nat. Photonics **6**, 525–528 (2012).
16. M. Wienold, L. Schrottke, M. Giehler, R. Hey, and H. T. Grahn, "Nonlinear transport in quantum-cascade lasers: The role of electric-field domain formation for the laser characteristics," J. Appl. Phys. **109**, 073112 (2011).
17. L. Schrottke, M. Giehler, M. Wienold, R. Hey, and H. T. Grahn, "Compact model for the efficient simulation of the optical gain and transport properties in THz quantum-cascade lasers," Semicond. Sci. Technol. **25**, 045025 (2010).
18. J. Ulrich, R. Zobl, N. Finger, K. Unterrainer, G. Strasser, and E. Gornik, "Terahertz-electroluminescence in a quantum cascade structure," Physica B **272**, 216–218 (1999).
19. S. Barbieri, J. Alton, C. Baker, T. Lo, H. E. Beere, and D. Ritchie, "Imaging with THz quantum cascade lasers using a Schottky diode mixer," Opt. Express **13**, 6497–6503 (2005).
20. R. Paiella, F. Capasso, C. Gmachl, D. L. Sivco, J. N. Baillargeon, A. L. Hutchinson, A. Y. Cho, and H. C. Liu, "Selfmode-locking of quantum cascade lasers with giant ultrafast optical nonlinearities," Science **290**, 1739–1742 (2000).
21. A. Gordon, C. Y. Wang, L. Diehl, F. X. Kärtner, A. Belyanin, D. Bour, S. Corzine, G. Höfler, H. C. Liu, H. Schneider, T. Maier, M. Troccoli, J. Faist, and F. Capasso, "Multimode regimes in quantum cascade lasers: From coherent instabilities to spatial hole burning," Phys. Rev. A **77**, 053804 (2008).
22. J. B. Khurgin, Y. Dikmelik, A. Hugi, and J. Faist, "Coherent frequency combs produced by self frequency modulation in quantum cascade lasers," Appl. Phys. Lett. **104**, 081118 (2014).
23. R. Lang, and K. Kobayashi, "External optical feedback effects on semiconductor injection laser properties," IEEE J. Quant. Electron. **QE-16**, 347–355 (1980).
24. G. Giuliani, M. Norgia, S. Donati, and T. Bosch, "Laser diode self-mixing technique for sensing applications," J. Opt. A: Pure Appl. Opt. **4**, S283-S294 (2002).
25. F. P. Mezzapesa, L. L. Columbo, M. Brambilla, M. Dabbicco, S. Borri, M. S. Vitiello, H. E. Beere, D. A. Ritchie, and G. Scamarcio, "Intrinsic stability of quantum cascade lasers against optical feedback," Opt. Express **21**, 13748–13757 (2013).
26. F. Keilmann, C. Gohle, and R. Holzwarth, "Time-domain mid-infrared frequency-comb spectrometer," Opt. Lett. **29**, 1542–1544 (2004).
27. G. Villares, A. Hugi, S. Blaser, and J. Faist, "Dual-comb spectroscopy based on quantum-cascade-laser frequency combs," Nat. Commun. **5**, 5192 (2014).
28. P. Gellie, S. Barbieri, J.-F. Lampin, P. Filloux, C. Manquest, C. Sirtori, I. Sagnes, S. P. Khanna, E. H. Linfield, A. G. Davies, H. Beere, and D. Ritchie, "Injection-locking of terahertz quantum cascade lasers up to 35 GHz using RF amplitude modulation," Opt. Express **18**, 20799–20816 (2010).

1. Introduction

Quantum-cascade lasers (QCLs) emitting in the terahertz (THz) spectral region are currently employed as light sources for various scientific applications, including heterodyne spectroscopy, gas sensing, tomography, coherent imaging, and metrology [1–8]. One of the drawbacks is their low operating temperature, which requires cryogenic cooling. However, compact table-top systems have been demonstrated based on the small but powerful mechanical Stirling coolers, which have become available in recent years [9, 10]. While for many applications single-mode operation is required, broad-band, multi-mode QCLs have recently gained a large interest. One reason for that is their ability to operate as frequency combs [11, 12] with many potential applications in the field of high-precision metrology and spectroscopy [13, 14]. One particular approach is the combination of a multi-mode THz QCL with an Echelle-type grating and a microbolometer focal-plane array in order to realize a fast, broad-band, high-resolution spectrometer for the THz range [3]. The resolution of such an instrument would be ideally limited by the intrinsic linewidth of the QCL, which has been found to be in the sub-kHz range for single-mode devices [15]. An ideal multi-mode source should exhibit a narrow linewidth for all modes in combination with a tuning behavior such that the total spectral range spanning over all the modes is continuously covered as a function of a certain control parameter. For multi-mode Fabry-Pérot ridge lasers, a continuous spectral coverage is expected for cavity lengths,

#214514 - $15.00 USD Received 6 Aug 2014; revised 2 Oct 2014; accepted 18 Nov 2014; published 1 Dec 2014

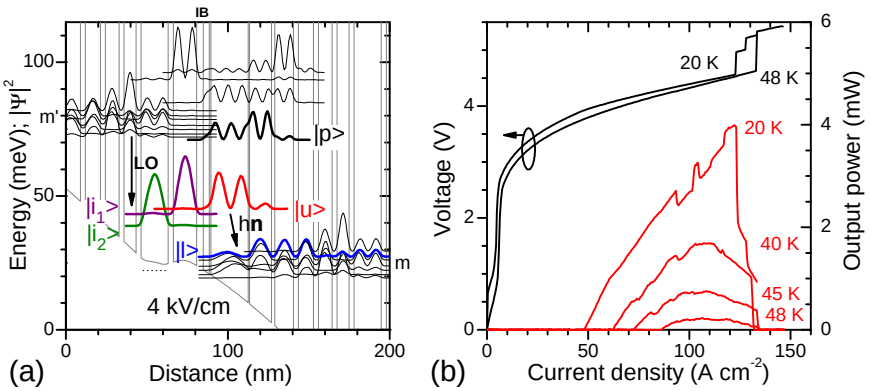

Fig. 1. (a) Calculated bandstructure diagram of the active region period at 4 kV/cm. The dashed line depicts the doped layer. $|i_1>$, $|i_2>$: injector states; $|u>$: upper laser level; $|p>$: parasitic state; $|l>$ lower laser level; IB: injection barrier; m, m′: minibands; LO: longitudinal optical phonon; $h\nu$: laser transition. (b) Light-current density-voltage characteristics under cw operation for the investigated 100 μm $\times$ 7.5 mm Fabry-Pérot laser.

for which the mode spacing becomes smaller than the individual tuning range of each modes. Since the mode tuning with current and temperature is of the order of 5 GHz for typical THz QCLs, this requires a cavity length of the order of 10 mm.

In this work, we investigated the spectral properties of such a long-cavity THz QCL. We start with the general properties of the QCL, followed by a discussion of its spectral characteristics with respect to frequency tuning and spectral coverage. Afterwards, we will discuss in more detail the different multi-mode operation regimes with a particular focus on frequency comb operation. In this manuscript, frequency comb operation refers to just the presence of a comb of equidistantly spaced modes as a consequence of the periodicity of the waveform at the round-trip frequency [11, 13]. It does not imply a full stabilization of the comb as required for metrological applications.

2. Active-region design and laser performance

In order to avoid excessive heat generation during cw operation, we employ an active region which features an ultra-low threshold current density in combination with low operating voltages. The active region of the QCL is based on a GaAs/$Al_{0.25}Ga_{0.75}As$ heterostructure with nine quantum wells per period and 85 periods as described in [16]. In Fig. 1(a), a band structure diagram is shown. Electrons are injected from the upper miniband m′ into the injector states $|i_1>$ and $|i_2>$ by exploiting fast longitudinal-optical phonon scattering. Electrons are then transfered into the upper laser state $|u>$ by resonant tunneling. Population inversion is achieved between state $|u>$ and the states of the lower miniband m, where the largest dipole matrix element occurs for the transition between $|u>$ and $|l>$. Active-region simulations as described in [17] show a gain maximum at 4.7 THz for this structure, although devices emit around 4.2 THz. The transition between the upper laser state $|u>$ and the parasitic state $|p>$ causes strong absorption around 6 THz, which results in a slightly asymmetric shape for the gain. State $|p>$ might also play a role for optical nonlinearities related to frequency comb operation. With respect to its electronic properties, one particular feature of this structure is the rather weak coupling between states on either side of the injection barrier, which explains the low operating current densities. The electronic properties, in particular the role of negative differential resistance (NDR) for this design, are discussed in detail in [16].

#214514 - $15.00 USD Received 6 Aug 2014; revised 2 Oct 2014; accepted 18 Nov 2014; published 1 Dec 2014

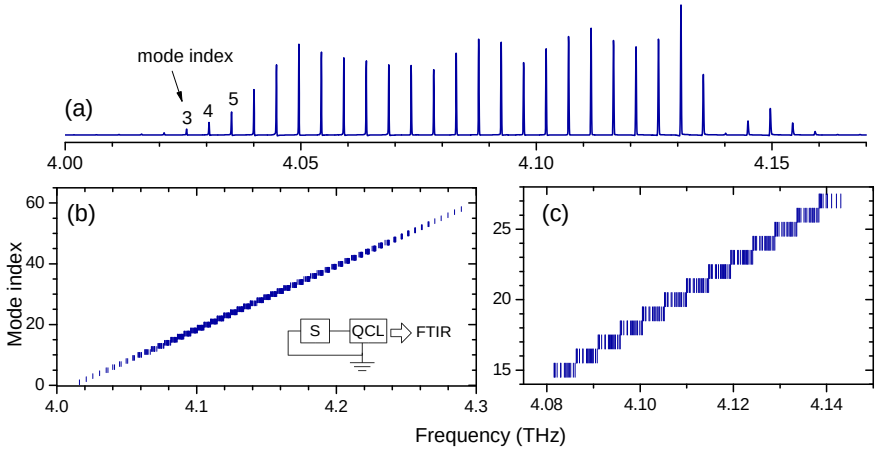

Fig. 2. (a) Multimode emission spectra for cw operation at 500 mA and 25 K. (b) Merged plot of the emission frequency vs. mode index for various cw operation conditions (20–50 K, 0.50–0.92 A). Inset: setup scheme; S: current source. (c) Magnification of the region, for which the tuning range of the individual laser modes becomes as large as the mode spacing of approximately 4.75 GHz (0.16 cm^{-1}).

In the following, we will discuss the experimental results for a 100 μm wide and 7.5 mm long Fabry-Pérot laser ridge based on a single-plasmon waveguide as first described in [18]. The continuous-wave (cw) light-current density-voltage characteristics are shown in Fig. 1(b) for several temperatures. The laser operates in cw mode up to approximately 50 K with an operating current range of 0.37–0.92 A (48–122 A cm^{-2}) at 20 K and a corresponding driving power of 1.5–4 W. The maximum output power is 4 mW at 20 K. For the present device, we did not observe any signature of electric-field domain formation below a current density of 122 A cm^{-2}, i.e. within the whole operating range exploited for this work.

3. Spectral characteristics

In order to characterize the emission, we used a high-resolution Fourier-transform infrared spectrometer (FTIR), which features a resolution of 0.0035 cm^{-1} or approximately 100 MHz (Bruker, IFS120). In addition, we studied the radio frequency (RF) beat note (BN) signal, which arises from multi-mode operation. The BN signal is measured by detecting the ac component of the QCL terminal voltage with an electrical spectrum analyzer (ESA), which allows for analyzing RF signals up to 26 GHz (Rohde & Schwarz, FISQ 26). In this configuration, the QCL acts not only as a source, but also as a fast detector for the beating signal of different spectral modes [19]. The effect can be ascribed to optical rectification of the strong cavity laser field at the metal/semiconductor interfaces. In contrast to optical measurements, which are limited by the resolution of the FTIR, the BN signal can be studied in principle with Hz-level resolution determined by the linewidth of the local oscillator of the ESA.

Before discussing the BN measurements, we will first characterize the tuning behavior as observed with the FTIR. In Fig. 2(a), one lasing spectrum for cw operation at 500 mA and 25 K is shown as an example. In order to estimate the spectral tuning range for each mode, we evaluated such spectra for different cw operating conditions. Each mode has been assigned to a mode index. Figure 2(b) depicts in a merged plot the mode index vs. the peak frequency of the individual laser modes for the whole current and temperature operating range. We find that the total emission range of the QCL spans 4.02–4.29 THz (135–144 cm^{-1}), while in the range

#214514 - $15.00 USD Received 6 Aug 2014; revised 2 Oct 2014; accepted 18 Nov 2014; published 1 Dec 2014

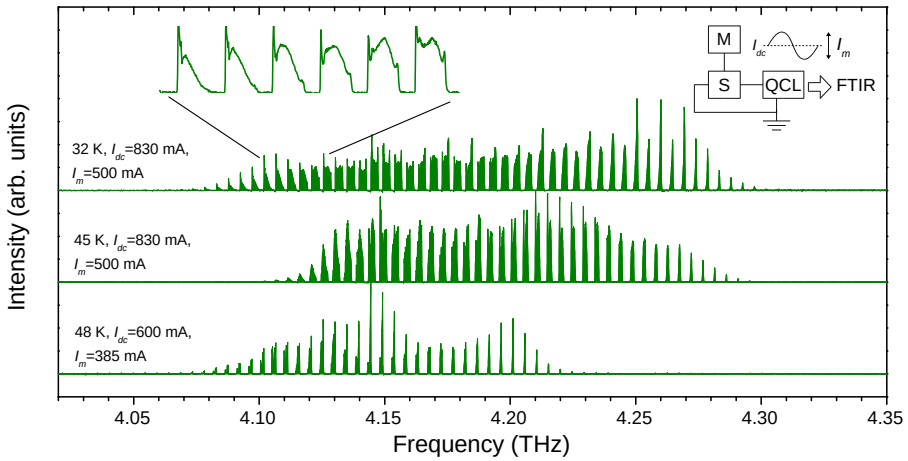

Fig. 3. Spectra under current modulation for different driving conditions (I_{dc}: nominal direct current, I_m: current modulation amplitude). To illustrate the spectral coverage, the area under the spectral peaks in the main graph is filled with color. Inset: setup scheme; M: modulation signal source (sinusoidal voltage).

of 4.08–4.14 THz (137–139 cm^{-1}) the tuning gaps between adjacent modes disappear [cf. Fig. 2(c)].

The data shown in Figs. 2(b) and 2(c) have been obtained from a large number of spectra measured under various operating conditions. In order to demonstrate also a fast tuning scheme as required for practical applications, we exploited the modulation function of the current source (Lightwave, LDX3232). For the spectra shown in Fig. 3, the direct driving current I_{dc} has been modulated with an amplitude I_m at several kHz. Since the time constant of the employed detector is long compared to the modulation speed, the measured spectra represent a temporal average. The apparent width of each mode represents its total tuning range under the specific modulation conditions, while the apparent line shape of each mode reflects the spectral power density and can exhibit rather individual features. The maximum spectral coverage of single laser modes under this scheme is about 3.1 GHz or 65% of the mode spacing. However, a continuous coverage between adjacent modes is obtained by performing such modulation measurements at different temperatures. From the data shown in Figs. 2 and 3, we infer a continuous spectral coverage for this device in the range of 4.08–4.14 THz (137–139 cm^{-1}) by a combination of current and temperature tuning.

In the following, we will classify the emission by its BN signature, while operating the QCL at a constant current and temperature. We refer to signals at the mode spacing frequency and twice the mode spacing frequency as f_{rt}-BN and $2f_{rt}$-BN, respectively, where f_{rt} stands for the round-trip frequency. To explain the origin of these two signals, we consider an optical pulse travelling through the cavity at the round-trip frequency $f_{rt} = c/(2Ln_g)$, where c denotes the vacuum speed of light, L the cavity length and n_g the group index. If the intensity of this pulse would remain constant along the cavity, no BN component should be present in the QCL terminal voltage since the voltage component due to the rectified optical field would be unmodulated in time. However, the pulse experiences gain within the cavity and mirror losses at the front and back facet of the laser ridge resulting in an intensity modulation along the cavity. Since the pulse passes the cavity twice during one round trip, a signal at $2f_{rt}$ is expected. More precisely: for cavities with a longitudinal mirror symmetry, only Fourier components at even multiples

#214514 - $15.00 USD Received 6 Aug 2014; revised 2 Oct 2014; accepted 18 Nov 2014; published 1 Dec 2014

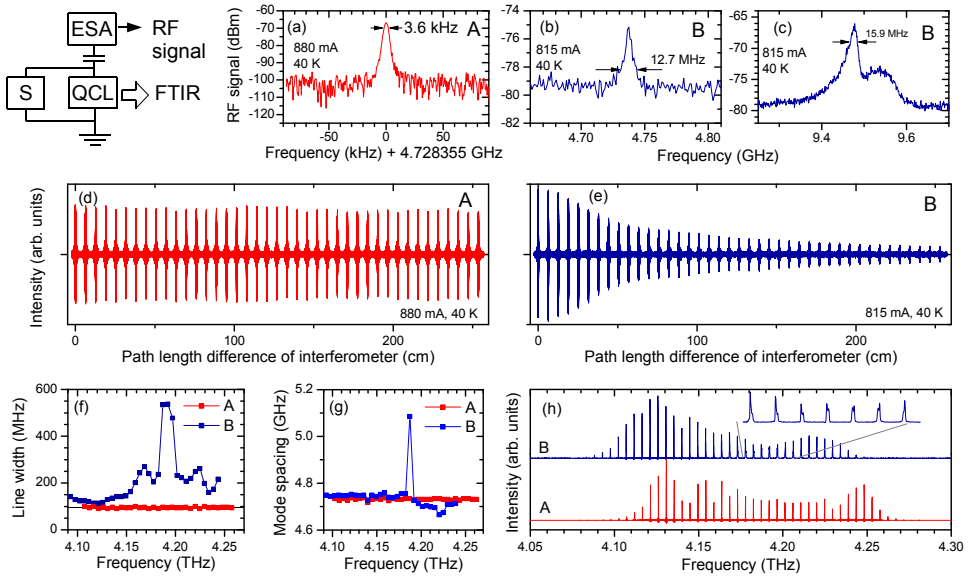

Fig. 4. (a) RF signal of the f_{rt}-BN for case A obtained at 880 mA and 40 K. The arrows indicate the 3 dB width. (b) RF signal of the f_{rt}-BN and (c) the $2f_{rt}$-BN for case B obtained at 815 mA and 40 K. (d) FTIR interferogram for case A. (e) FTIR interferogram for case B. (f) Linewidth vs. frequency (full width at half maximum) corresponding to (d) and (e). The resolution limit of the FTIR is depicted as a solid line. (g) Mode spacing vs. frequency and (h) intensity spectra corresponding to (d) and (e).

of f_{rt} contribute to the electrical BN signal, where the strongest component occurs at $2f_{rt}$ if the waveform emitted from one facet is modulated at f_{rt}. Electrical BN signals at f_{rt} and odd multiples of it are due to small asymmetries, which are always present in true devices.

Depending on the operating conditions, different situations are observed for the BN signal, which are related to different optical signatures revealed by high-resolution FTIR spectroscopy. The two main cases, labeled A and B, are illustrated in Fig. 4. Case A is characterized by the presence of a narrow f_{rt}-BN [cf. Fig. 4(a)] as well as a narrow $2f_{rt}$-BN (not shown), while case B is characterized by broad f_{rt}- and $2f_{rt}$-BNs [cf. Figs. 4(b) and 4(c)]. We did not observe BN signals corresponding to any higher multiple of the mode spacing frequency, which we explain by the stronger damping of such high frequencies in the employed configuration and the limitation of the ESA to frequencies below 26.5 GHz. In case A, the observed narrow f_{rt}- and $2f_{rt}$-BN signals have a 3 dB width of only a few kHz. The peak amplitudes in the corresponding FTIR intensity interferogram remain almost constant with increasing path length difference of the two interferometer arms [cf. Fig. 4(d)]. The observed optical linewidth is set by the resolution of the FTIR for all modes [cf. Fig. 4(f)]. In case B, the f_{rt}- and $2f_{rt}$-BNs [cf. Figs. 4(b) and 4(c)] have a 3 dB width of several MHz. The $2f_{rt}$-BN exhibits an additional spectral feature next to the main peak and can be detected within a range as large as 200 MHz. We explain the observed differences between the f_{rt}- and $2f_{rt}$-BNs by the much larger signal amplitude of the $2f_{rt}$-BN (also observed in case A), which provides a better discrimination of the background noise. In case B, the peak amplitudes in the intensity interferogram show a clear decay with increasing path length difference [cf. Fig. 4(e)]. This decay is correlated with an increase of the apparent optical linewidth of the spectral modes [cf. Fig. 4(f)], which can be of the order of several hundred MHz — well above the resolution of our FTIR. In Fig. 4(g), the mode spacing is com-

#214514 - $15.00 USD Received 6 Aug 2014; revised 2 Oct 2014; accepted 18 Nov 2014; published 1 Dec 2014

pared for the two cases. For case A, all the modes are found to be equidistantly spaced (within the instrumental limitations), while in case B a deviation from an equidistant mode spacing is observed for a part of the emission spectrum. As illustrated in Fig. 4(h), cases A and B can exhibit similar spectral envelopes. However, a closer look at the spectrum in case B reveals a superposition of closely spaced modes in the spectral range for which the strongest deviations from an ideally measured comb spectrum (with respect to linewidth and mode spacing) are observed. Note that no current modulation has been applied. Hence, the observed deviations from an ideal comb spectrum are intrinsic in case B. While the presence of broad BN regimes has already been reported for mid-infrared and THz QCLs [11, 12], a satisfying physical explanation for this case is still lacking. Our measurements employing a high-resolution FTIR point to a rather complex behavior — an explanation just by gain saturation and the presence of group velocity dispersion (GVD) might be to simplistic. We explain the observation of narrow BN signals in case A by frequency comb operation, for which mode coupling due to a nonlinear optical mechanism results in an equidistant mode spacing. In the following, we will provide further evidence for a coherent coupling of the modes in type-A regimes as expected for true frequency comb operation.

4. Frequency comb operation in the presence of weak external optical feedback

The observation of multi-mode emission in combination with a narrow BN signal for mid-infrared QCLs has been originally associated with self-mode locking [20] and later in a more general frame with frequency comb operation of QCLs [11]. Both explanations imply that the individual modes are locked with each other resulting in an equidistant mode spacing. In the presence of a dispersive waveguide, this requires a nonlinear optical mechanism which couples the modes and compensates the GVD. Potential candidates for such a mechanism include spatial hole burning in the presence of a saturable absorber [21] and four-wave mixing due to the third-order intersubband susceptibility [11, 22]. Depending on the particular phase relation between the locked modes, the temporal output characteristics can range between the extreme cases of ultrashort pulses and a constant output intensity. Irrespective of the particular nonlinear mechanism, we expect mode locking to be facilitated in long cavities due to the smaller mode spacing and consequently the smaller group velocity differences between the Fabry-Pérot modes of the cold cavity, i.e. the cavity without gain and photons.

The absence of suitable autocorrelation setups and high-resolution etalons for the mid-infrared and terahertz range makes it difficult to directly verify frequency comb operation for QCLs. Although the observation of regularly spaced modes in combination with a narrow BN is already a strong indication for frequency comb operation, it has been argued that this is not sufficient as a proof. In the pioneering paper on QCL-based frequency combs [11], it has been pointed out that also a single pair of modes might cause the narrow BN signal. In order to verify frequency comb operation, one has to show that indeed a large number of optical modes contribute to the BN signal. Such an indirect proof for frequency comb operation is provided by optically resolved measurements of the BN signal. So far, techniques include so-called intermode beat spectroscopy [11] or shifted-wave interference Fourier-transform (SWIFT) spectroscopy [12]. Both techniques have in common that they are experimentally rather challenging, requiring ultrafast detectors and/or sophisticated setups. The technique, which we will describe here, exploits the sensitivity of QCLs to external optical feedback (EOF), namely the self-mixing effect, and requires not much more than an ESA and a movable mirror, where in the latter case we will exploit the moving mirror of the FTIR interferometer.

The behavior of diode lasers under EOF has been studied for several decades, starting with the seminal paper of Lang and Kobayashi [23]. In the case of strong feedback, a rich spectrum of effects related to nonlinear dynamics is observed, which constitutes a whole field of research in its own. In the weak-feedback regime, the sensitivity of single-mode diode lasers (as well

#214514 - $15.00 USD Received 6 Aug 2014; revised 2 Oct 2014; accepted 18 Nov 2014; published 1 Dec 2014

as QCLs) to EOF can be exploited for interferometric sensors based on the self-mixing effect [6, 24, 25]. Except for the statement that EOF should be avoided for frequency comb operation [11], there is currently little known about EOF-related effects in multi-mode QCLs. In our case, we did not observe EOF-related effects for the broad-BN regime, while we found that the QCL reacts sensitively to EOF in the narrow-BN regime. If in the latter case the EOF is sufficiently weak, we observe a shift of the BN frequency, which depends on the intensity and phase of the EOF. For strong EOF, additional nonlinear effects are observed such as the splitting into multiple BNs, which goes beyond the scope of this paper. We found that the presence of EOF can also cause artifacts in the measured optical spectra, such as weak sidebands next to the main comb and spectral replica at higher harmonics and subharmonics. These artifacts are much more pronounced for narrow-BN regimes due to the sensitivity of the QCL to EOF in this case. In order to suppress feedback-related artifacts in the measured spectra, we employed a broad-band optical attenuator placed in front of the cryostat windows. To convince ourselves that residual EOF does not corrupt the optical spectra, we attenuated the intensity until a further attenuation did not change the spectra, except for a smaller intensity. By employing an attenuation of 90%, the residual artifacts are below the level caused by detector nonlinearities. The residual EOF from the FTIR results then in an alternating frequency shift of the BN, which is of the order of 100 kHz and correlated with the motion of the moving mirror of the FTIR interferometer.

There exists currently no satisfying theoretical model describing multi-mode operation of QCLs in the presence of EOF. Nevertheless, with some intuitive physical assumptions, one can derive an expression from the Lang-Kobayashi (LK) model for diode lasers [23], which describes our experimental findings for weak EOF very well. The idea is the following: For a single-mode laser, weak EOF results in a shift of the laser frequency. Considering two independent laser modes with indices m and n, the individual frequency shift for each mode results in a variation of the beating frequency $\delta\omega_{mn}$. In general, $\delta\omega_{mn}$ differs for each pair of modes. However, in the case of a frequency comb, the modes are coupled and equidistantly spaced, and consequently $\delta\omega_{mn}$ must be the same for all pairs of adjacent modes. One can think now of two scenarios: first, the mode coupling results in a collective shift of the BN frequency under EOF or, alternatively, EOF simply destroys the frequency comb. Since only the former is consistent with our experimental findings for weak EOF, it is reasonable to assume that the observed variation of the BN frequency is a collective phenomenon caused by all the involved mode pairs. By taking into account contributions from all pairs of adjacent modes, one obtains the following expression for the shift $\delta\omega_{\mathrm{BN}}$ of the beating frequency:

$$\delta\omega_{\mathrm{BN}}(\tau) = \sum_{i=1}^{N} a_i \sin(\omega_i \tau + \theta_i)\,, \tag{1}$$

where τ denotes the EOF delay time, N the number of modes, ω_i the frequency of the laser mode with index i and a_i as well as θ_i real-valued constants. Equation (1) can be seen as a rather general form of an interferogram, where the path length difference is simply $c\,\tau$. In contrast to the usual intensity interferograms obtained with an FTIR, $\delta\omega_{\mathrm{BN}}(\tau)$ contains also non-trivial phase information via θ_i, which reflects the mode pair coupling and which is therefore not directly linked to the optical phase. Indeed, Eq. (1) is a short-hand notation for a sum over contributions from all pairs of adjacent modes. A detailed formal motivation for Eq. (1) is given in the Appendix A. In the following, we call $\delta\omega_{\mathrm{BN}}(\tau)$ the BN interferogram.

5. Beat note spectroscopy based on the self-mixing effect

In order to measure a BN interferogram, we exploit the real-time demodulation function of the ESA in combination with the well-defined position of the moving mirror of the FTIR interferometer. The configuration of the ESA is the same as for listening to an FM radio channel (mono) at the BN frequency. The analog signal present at the audio output of the device is

#214514 - $15.00 USD Received 6 Aug 2014; revised 2 Oct 2014; accepted 18 Nov 2014; published 1 Dec 2014

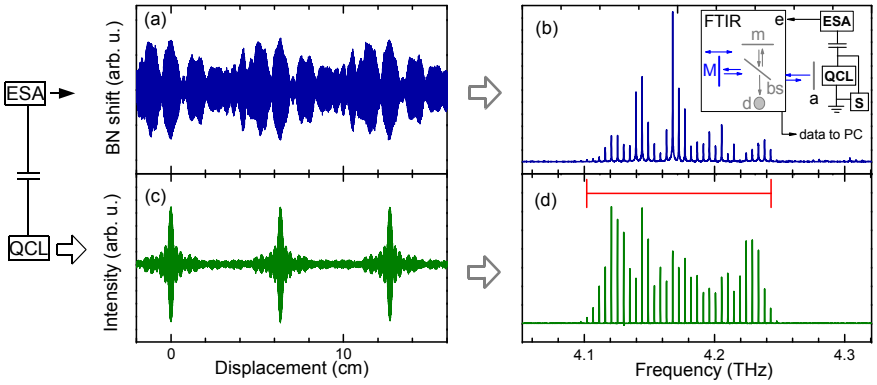

Fig. 5. (a) Beat note interferogram (BN frequency shift vs. displacement of the moving FTIR mirror) of the f_{rt}-BN for cw operation at 843 mA and 40 K. (b) Power spectrum corresponding to (a). Inset: scheme of the measurement setup. M: moving mirror; m: stationary mirror; bs: Ge-coated mylar beam splitter; d: pyroelectric detector; a: broad-band attenuator (several sheets of paper); e: external detector input. (c) FTIR intensity interferogram (intensity vs. interferometric path length difference) for the same operating conditions as in (a). (d) Optical intensity spectrum corresponding to (c). The red line indicates the range of the optical spectrum.

fed into the external detector input of the FTIR. Since the real-time demodulation bandwidth of our ESA is limited to 200 kHz, the optical feedback had to be attenuated to less than 1%. A BN interferogram is shown in Fig. 5(a), and a scheme of the setup is depicted in the inset of Fig. 5(b). The BN interferogram is conveniently recorded by using the standard rapid scan mode of the FTIR; no step scan technique is needed. However, a sufficient stabilization of the temperature and current is required in order to avoid a drift of the BN frequency beyond the bandwidth of the demodulator during the measurement. To our experience, the temperature has to be maintained at a constant value within a few mK, and the current source has to be kept on the desired current level for several minutes prior to starting the measurement. We ascribe the measured modulation of the BN frequency to the coherent, i.e. phase-sensitive, nature of EOF. An direct experimental verification for the coherent nature of the self-mixing signal is presented in Appendix B. Figure 5(b) depicts the power spectrum corresponding to Fig. 5(a) showing the frequency components, which contribute to the BN. Figures 5(c) and 5(d) depict the conventional FTIR intensity interferogram and the corresponding QCL emission spectrum, respectively, obtained under the same operating conditions as for Fig. 5(a). From a comparison of the BN spectrum with the QCL emission spectrum, we see that virtually all modes which are present in the emission spectrum contribute also to the narrow BN. Hence, we consider the observed behavior as a proof for stable frequency comb operation. The envelope of the BN spectrum in Fig. 5(b) differs from that of the optical intensity spectrum in Fig. 5(d), since the amplitude as well as the phase (not shown) of the BN spectrum originate mainly from mode pair interactions. The periodicity within the phase-sensitive BN interferogram can be seen as a direct consequence of the periodicity of the optical waveform at the round-trip frequency, which implies equidistantly spaced modes, i.e. frequency comb operation. A direct argument for the phase-sensitive nature of the BN interferogram is the following: phase-insensitive intensity interferograms require the symmetry of the envelope around a point of zero path difference. For a phase-insensitive interferogram, a periodic envelope implies therefore also the symmetry with respect to each maximum, which is incompatible with the asymmetric period of the BN interferogram.

#214514 - $15.00 USD Received 6 Aug 2014; revised 2 Oct 2014; accepted 18 Nov 2014; published 1 Dec 2014

The presence of frequency comb operation does, by itself, not tell us anything about the time dependence of the emission. Depending on the physical mechanism of mode locking, the time dependence can in principle range between the two extreme cases: a flat intensity in time and ultrashort pulses. In the case of ultrashort pulses, we would expect a feedback signal only for EOF delay times for which the feedback pulse coincides with the laser pulse inside the cavity. Therefore, the BN interferogram should exhibit sharp peaks, which are periodically separated by c/f_{rt}. Hence, we exclude the presence of ultrashort pulses in case of Fig. 5.

One might ask the question, to which extent the stationary mirror in the FTIR contributes to the BN interferogram in Fig. 5(a), since it is a major component for obtaining the usual intensity interferograms. With respect to the BN interferogram, it constitutes a stationary source of external feedback as there are several others such as reflections at the windows. The main point here is that these sources create stationary feedback terms, which result in a constant shift of the BN frequency. Since only components are detected which vary with the position of the moving mirror, these stationary terms are not relevant for the measurement. This assumption can be made as long as the EOF is sufficiently weak so that the system remains in the linear regime, for which the different contributions are independent of each other. The validity of this interpretation has been confirmed by performing a control measurement with a single mirror mounted on a linear translation stage. The results shown in Appendix B confirm that the recording of BN interferograms does not rely on the stationary mirror of the FTIR. BN interferograms recorded with a single mirror are qualitatively similar to the one shown in Fig. 5(a) using the FTIR setup (cf. Appendix B).

In contrast to interferometric sensors based on the self-mixing effect of single-mode lasers, the presented technique is not affected by low-frequency noise (which is negligible at GHz frequencies) and does therefore not require lock-in techniques. Hence, the measurement principle constitutes a fast coherent detection scheme, which might be employed for further applications.

6. Stability of the beat note under variation of the bias current

One important aspect of frequency comb operation is the stability of the comb with respect to control parameters such as current and temperature. We already identified two operating regimes A and B, corresponding to the presence of a narrow and a broad BN, respectively. Figures 6(a) and 6(b) depict maps of the f_{rt}- and $2f_{rt}$-BN signals as a function of the current, while maintaining a constant temperature. The maps consist of subsequently recorded BN traces, where each trace has been acquired for a constant current value. Stable comb operation is likely obtained only for regions in which a single narrow BN is present at f_{rt} and $2f_{rt}$ (case A), while quasi-stable comb operation, i.e. a superposition of two or more combs, might be obtained in regions with several narrow BNs (case A1). In the presence of several sub-combs, qualitative differences between the f_{rt}- and $2f_{rt}$-traces are expected since then the spacing between modes separated by twice ore more the Fabry-Pérot interval is not always an exact multiple of the spacing between adjacent modes. Another reason for differences in both traces is the much larger signal amplitude of the $2f_{rt}$-BN revealing features which are below the noise floor in the f_{rt}-BN. We also encountered situations in which only a narrow $2f_{rt}$-BN was present. In these situations, every second mode was suppressed in the FTIR intensity spectra (not shown). For the regions in Figs. 6(a) and 6(b) exhibiting a broad BN (case B), no stable frequency comb operation is expected. As discussed above, this regime is also related to a significant broadening of the optical lines (cf. Fig. 4). There are also several other regions, for which the BN signal exhibits more complex signatures and cannot be classified into one of the discussed cases. However, as in case B, we do not expect stable frequency comb operation in these situations. The data shown in Fig. 6 have been recorded with the same setup as used for the optical measurements except for blocking the beam. Therefore, a certain EOF from stationary reflections inside the optical cryostat is always present. Since EOF is one of the main origins for complex non-

#214514 - $15.00 USD Received 6 Aug 2014; revised 2 Oct 2014; accepted 18 Nov 2014; published 1 Dec 2014

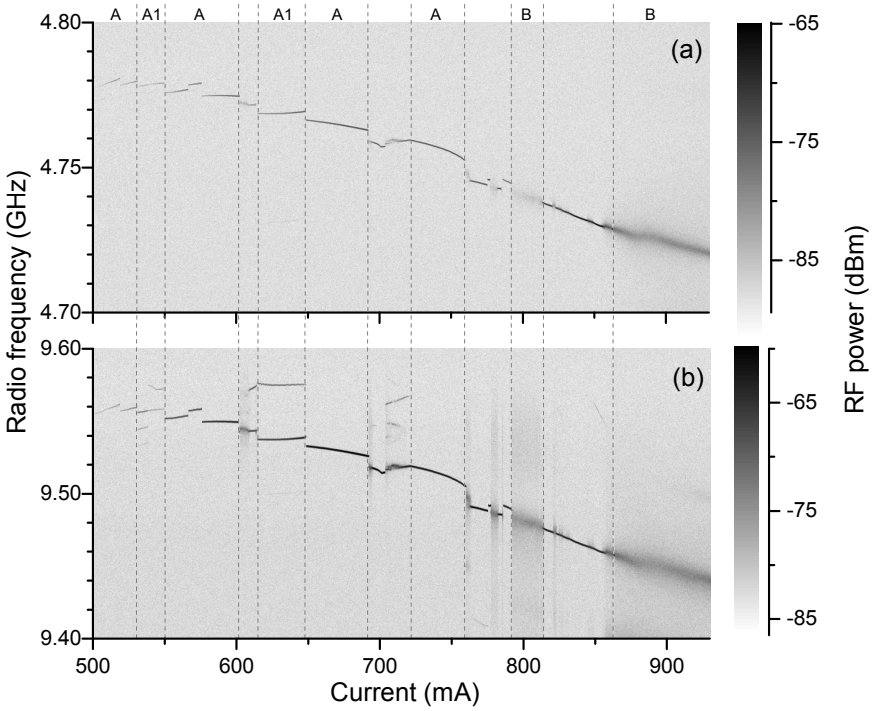

Fig. 6. (a) Spectral map of the f_{rt}-BN signal under variation of the current at 40 K (0.5 mA step size). (b) Map of the $2f_{rt}$-BN signal. The vertical dashed lines have been added in order to indicate the different BN regimes.

linear dynamical effects in semiconductor diode lasers [23], one question is to which extent the observed dynamical behavior is induced by the remaining stationary EOF in our case. In order to avoid any kind of EOF, we placed another QCL between two slabs of absorbing material (Eccosorb). However, we still observed narrow- and broad-BN regimes as well as transition regions showing features of both (not shown). Note that the details of the BN characteristics as shown in Fig. 6 can be very sensitive to the measurement conditions. In particular, regions in which several narrow beat notes coexist are very fragile and usually not robustly repeated in consecutive measurements. Another implication of the behavior shown in Fig. 6 arises from the discontinuities of the BN frequency as a function of the current. Although not directly observable with the FTIR, we exclude that the optical modes experience a continuous frequency tuning on a MHz and sub-MHz scale, while the BN signal exhibits discontinuities as a function of the control parameter.

What are the consequences of the observed dynamical behavior with respect to using such a QCL as a spectroscopic source? First, for operation at a constant bias current and temperature, the described dynamical behavior will probably be of minor importance as long as suitable operating parameters are chosen. Such an application based on two QCLs could be dual-comb spectroscopy [26, 27] although this might require additional active stabilization measures. Second, if a resolution of several hundred MHz is acceptable, a single QCL employed as a broad-band source could be used for fast laser absorption spectroscopy within a grating setup as described in [3]. However, a much better resolution in such a configuration is expected if the the QCL operates in a frequency comb regime of type A and, within this range, the BN frequency remains a continuous function of the control parameters. Due to the complex dynamical behavior, a prac-

#214514 - $15.00 USD Received 6 Aug 2014; revised 2 Oct 2014; accepted 18 Nov 2014; published 1 Dec 2014

tical difficulty will be to identify such suitable parameter ranges in order to cover the desired absorption features.

We would like to emphasize that we did not try to compensate the GVD of the cavity such as in [11] and [12]. In the present case, the GVD of the cavity is solely compensated by the nonlinear optical mechanism which couples the modes. Due to the vicinity of the phonon absorption band, the GVD of the cold cavity is already quite strong around 4.2 THz, while it becomes weaker toward smaller THz frequencies. Hence, we believe that stable frequency comb regimes should be more easily obtained for QCLs emitting at somewhat smaller frequencies. With respect to frequency tuning, also active injection mode locking as in [28] might be exploited for broad band, long-cavity QCLs. However, we expect this to be a rather complex physical issue due to the many more scenarios in case of an additional RF injection signal.

7. Summary

We demonstrated a broad-band THz QCL, which exhibits several mW of continuous-wave output power, a total spectral coverage of 270 GHz (9 cm^{-1}) around 4.2 THz (139 cm^{-1}), as well as a continuous spectral coverage within a range of 60 GHz (2 cm^{-1}). We identified different multi-mode operating regimes by its RF beat note signature. We confirmed that the presence of a narrow beat note with an RF linewidth in the kHz range is related to frequency comb operation. For the presented long-cavity device, frequency tuning which exceeds the Fabry-Pérot mode spacing is obtained by varying the operating current and temperature. However, a continuous tuning in the frequency comb mode is only obtained within limited ranges of the bias current due to nonlinear dynamical effects. In the presence of a broad beat note, we found that the optical linewidth can exceed several hundred MHz, which will limit the use of such a source for high-resolution spectroscopy. We infer the drawbacks of the present device to the detrimental impact of the GVD, which has not been actively compensated. Since the GVD of the cold cavity decreases toward smaller frequencies, we believe that many of the current limitations can be avoided by realizing devices at somewhat lower THz frequencies, in particular, if additional means are used to compensate the cold-cavity GVD [12]. We further demonstrated an experimental technique to characterize QCL-based frequency combs relying on the self-mixing effect. The measurement principle might also pave the way toward fast and sensitive detection schemes employing QCL-based frequency combs.

#214514 - $15.00 USD Received 6 Aug 2014; revised 2 Oct 2014; accepted 18 Nov 2014; published 1 Dec 2014

Appendix A

In this Appendix, we would like to motivate Eq. (1). A basic approach to describe a semiconductor laser under external optical feedback is the Lang-Kobayashi (LK) model [23]. The LK equation is given by

$$c_g^{-1}\partial_t \mathscr{E}(t) = g(1+i\alpha)\mathscr{E}(t) + \kappa\mathscr{E}(t-\tau)\exp(-i\omega_0\tau) \; . \tag{2}$$

Here, $\mathscr{E}$ denotes the slowly varying envelope of the electric field E with $E(t) = \mathscr{E}(t)\exp(i\omega_0 t)$. Without the second term on the right-hand side, this resembles the laser equation in the adiabatic approximation, for which the polarization follows the electric field. c_g denotes the group velocity, g the net field gain, and α a factor, which reflects the coupling of the real and the imaginary part of the dielectric susceptibility and is closely related to the linewidth enhancement factor for diode lasers. κ denotes the feedback parameter, τ the delay time, and ω_0 the optical carrier frequency. For a single-mode laser, the usual approach is

$$\mathscr{E}(t) = \mathscr{E}_0\exp(i\delta\omega t) \; , \tag{3}$$

where $\mathscr{E}_0$ is a constant prefactor and $\delta\omega$ the frequency shift related to EOF. By separating real and imaginary terms of Eq. (2) and setting $c_g = 1$, one obtains

$$\delta\omega = \alpha g - \kappa\sin\left[(\delta\omega+\omega_0)\tau\right] \tag{4}$$

and

$$g = -\kappa\cos\left[(\delta\omega+\omega_0)\tau\right] \; . \tag{5}$$

Inserting Eq. (5) into Eq. (4) results in

$$\delta\omega = -C\sin\left[(\delta\omega+\omega_0)\tau+\phi\right] \; , \tag{6}$$

where $\phi = \arctan(\alpha)$ and $C = \kappa\sqrt{\alpha^2+1}$. In case of a sufficiently weak feedback and under the condition $\delta\omega\tau \ll \pi$, the implicit Eq. (6) can be approximated by the explicit equation

$$\delta\omega = -C\sin\left(\omega_0\tau+\phi\right) \; , \tag{7}$$

which can be exploited for interferometric measurements based on the self-mixing effect. To illustrate the situation in case of multi-mode operation, we consider now two independent modes ω_1 and ω_2. The BN frequency shifts due to optical feedback by the quantity

$$\delta\omega_{12} = \delta\omega_1 - \delta\omega_2 = C\left[\sin(\omega_2\tau+\phi) - \sin(\omega_1\tau+\phi)\right] \; . \tag{8}$$

Of course, just two modes do not represent a frequency comb, for which the condition

$$\delta\omega_{mn} = \delta\omega_{(m+1)(n+1)} \tag{9}$$

must be fulfilled for all mode pairs mn. It is not possible to strictly derive an equivalent expression for Eq. (8) within the LK model for three or more coupled modes. The problem is that Eq. (2) is not well suited to describe multi-mode operation in the presence of mode coupling, which is due to the neglected spatial dependence. Therefore, we follow here a different approach based on intuitive physical arguments. First, we rewrite Eq. (8) for a pair of adjacent modes with index i and $j = i+1$ as

$$\delta\omega_{ij} = \delta\omega_i - \delta\omega_j = C_{ij}\left[\sin(\omega_j\tau+\phi_{ij}) - \sin(\omega_i\tau+\phi_{ij})\right] \; , \tag{10}$$

where C_{ij} and ϕ_{ij} are individual parameters for each mode pair ij. We refer to $\delta\omega_{ij}$ as the LK shift of the mode pair ij, which is the shift of the difference frequency in the absence of mode

#214514 - $15.00 USD Received 6 Aug 2014; revised 2 Oct 2014; accepted 18 Nov 2014; published 1 Dec 2014

coupling. In general, the LK shift differs for each mode pair. However, from the experiments, we know that weak EOF results in a collective shift $\delta\omega_{\mathrm{BN}}$ of the BN frequency as a function of τ, which is explained by the presence of a mode coupling mechanism. We assume now that this collective shift is proportional to the average LK shift of all mode pairs plus a term representing the shift of the optical carrier frequency ω_0:

$$\delta\omega_{\mathrm{BN}} \sim \delta\omega_0 + \sum_{i=1}^{N-1} \delta\omega_{ij} = C_0 \sin(\omega_0\tau + \phi_0) + \sum_{i=1}^{N-1} C_{ij}[\sin(\omega_j\tau + \phi_{ij}) - \sin(\omega_i\tau + \phi_{ij})] \,, \quad (11)$$

where the averaging factor $1/N$ is contained in the constant of proportionality. Note that for a frequency comb the carrier frequency ω_0 is equal to one of the comb frequencies ω_i. Equation (11) can therefore be written as

$$\delta\omega_{\mathrm{BN}}(\tau) = \sum_{i=1}^{N} a_i \sin(\omega_i\tau + \theta_i) \quad (12)$$

which is Eq. (1). Indeed, we find that the measured BN interferograms are very well described by the last equation with real-valued coefficients a_i and θ_i. These coefficients are obtained from the complex Fourier components of the BN interferogram at the emission frequencies ω_i. Note that θ_i is not directly related to the optical phase of the modes. According to Eq. (11), the coefficients a_i and θ_i reflect the mode-pair coupling in the QCL. In principle, a reconstruction of this information, i.e. of the coefficients C_0, ϕ_0, C_{ij}, and ϕ_{ij}, should be possible from the measurements. However, to avoid phase errors, the delay time τ would have to be known with absolute precision.

Appendix B

In this Appendix, we present a direct experimental evidence for the phase-sensitive nature of the proposed self-mixing BN spectroscopy. Therefore, we performed measurements in the absence of the FTIR beam splitter. Since the FTIR cannot be exploited for the BN spectroscopy in this case, we employed a plane mirror mounted on a motorized linear translation stage. A sketch of the experimental configuration is shown in the right inset of Fig. 7(a). The data acquisition is similar to the original method described in section 5 except that the analog to digital conversion of the audio signal takes place via a digital multimeter (Keithley, Model 2002). Figure 7(a) depicts a recorded BN power spectrum, where the corresponding BN interferogram is shown in the left inset. The presence of several experimental shortcomings prevented measurements over a larger delay path, which would allow for a resolution of the individual modes in the power spectrum. Figure 7(b) depicts the emission spectrum as measured with an FTIR and an incoherent DTGS detector. Note that the individual modes are also not resolved here. The corresponding FTIR interferogram is shown in the inset of Fig. 7(b). The width of the emission spectrum coincides with that of the BN power spectrum, which demonstrates that modes over the whole emission range contribute to the narrow BN. However, the main point here is that, in the absence of an interferometric intensity modulation, BN spectroscopy would not be possible for an incoherent detection mechanism.

#214514 - $15.00 USD Received 6 Aug 2014; revised 2 Oct 2014; accepted 18 Nov 2014; published 1 Dec 2014

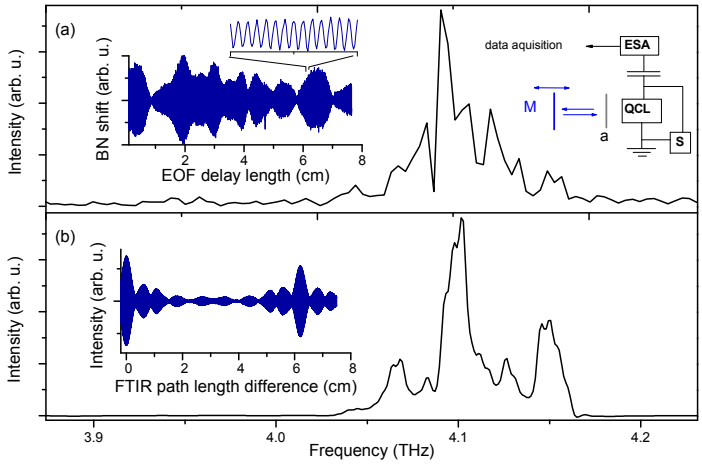

Fig. 7. Results for BN spectroscopy with a single mirror and FTIR measurements for a 100 μm $\times$ 7.4 mm Fabry-Pérot laser operated in a narrow BN regime at 543 mA and 30 K. (a) Power spectrum obtained from the BN interferogram. Left inset: corresponding BN interferogram (FM signal amplitude vs. EOF delay length). Note that the zero position of the delay axis is offset by several cm from the position of the front facet. Right inset: experimental setup. ESA: electrical spectrum analyzer; S: current source; a: attenuator. (b) Emission spectrum recorded with a Bruker, IFS66v FTIR for the same operating conditions. Inset: corresponding FTIR interferogram.

Acknowledgments

The authors would like to thank R. Hey and M. Höricke for sample growth, W. Anders for sample processing, and G. Rozas for helpful discussions.

#214514 - $15.00 USD Received 6 Aug 2014; revised 2 Oct 2014; accepted 18 Nov 2014; published 1 Dec 2014